

Fossil AGN jets as ultra high energy particle accelerators

Gregory Benford^{1*}, R. J. Protheroe^{2†}

¹*Department of Physics and Astronomy, University of California, Irvine, CA 92697-4575, USA*

²*Department of Physics, School of Chemistry & Physics, University of Adelaide, Adelaide, SA 5005, Australia*

27 October 2018

ABSTRACT

Remnants of AGN jets and their surrounding cocoons leave colossal magnetohydrodynamic (MHD) fossil structures storing total energies $\sim 10^{60}$ erg. The original active galactic nucleus (AGN) may be dead but the fossil will retain its stable configuration resembling the reversed-field pinch (RFP) encountered in laboratory MHD experiments.

In an RFP the longitudinal magnetic field changes direction at a critical distance from the axis, leading to magnetic re-connection there, and to slow decay of the large-scale RFP field. We show that this field decay induces large-scale electric fields which can accelerate cosmic rays with an E^{-2} power-law up to ultra-high energies with a cut-off depending on the fossil parameters. The cut-off is expected to be rigidity dependent, implying the observed composition would change from light to heavy close to the cut-off if one or two nearby AGN fossils dominate. Given that several percent of the universe's volume may house such slowly decaying structures, these fossils may even re-energize ultra-high energy cosmic rays from distant/old sources, offsetting the “GZK-losses” due to interactions with photons of the cosmic microwave background radiation and giving evidence of otherwise undetectable fossils. In this case the composition would remain light to the highest energies if distant sources or fossils dominated, but otherwise would be mixed. It is hoped the new generation of cosmic ray experiments such as the Pierre Auger Observatory and ultra-high energy neutrino telescopes such as ANITA and lunar Cherenkov experiments will clarify this.

Key words: acceleration of particles – MHD – magnetic fields – galaxies: active – galaxies: jets – intergalactic medium

1 INTRODUCTION

The energy spectrum of cosmic rays (CR) extends from below 1 GeV up to at least 10^{20} eV. The bulk of the cosmic rays below $\sim 10^{18}$ eV are probably Galactic. It is currently unknown whether the ultra-high energy (UHE) cosmic rays are Galactic or extragalactic in origin, and whether they are accelerated or result from emission by topological defects or decay of super-massive particles. If they are accelerated, they are almost certainly extragalactic in origin. This is because their gyroradii are sufficiently large that an anisotropy would be expected toward a galactic source population (not observed), and because there are no obvious Galactic source populations having magnetic fields such that gyroradii of UHE CR are compatible with their size.

Possible extragalactic acceleration sites include hotspots of giant radio galaxies, the intergalactic medium, gamma ray bursts and blazar jets. Extragalactic CR at

the highest energies are, however, subject to interaction with the cosmic microwave background radiation (CMBR). In the rest frame of a UHE CR proton, photons of the 2.73 K CMBR are strongly blue-shifted to gamma-ray energies. The thresholds for Bethe-Heitler pair production and pion photo-production by UHE CR protons on the CMBR are close to 2×10^{17} eV and 2×10^{19} eV, respectively. Protons at 3×10^{19} eV and 3×10^{20} eV typically lose a large fraction of their energy in a time of 1 Gpc/c (3×10^9 y) and 10 Mpc/c (3×10^7 y), respectively. The importance of pion photoproduction on the CMBR was first noted by Greisen (1966) and Zatsepin & Kuzmin (1966) and the cut-off they predicted is referred to as the “GZK cut-off”. The pion photoproduction interactions result in a flux of UHE neutrinos, often referred to as “GZK neutrinos”, which would point back to halos surrounding the UHE cosmic ray sources. Several experiments (Takeda et al. (2003), Bird et al. (1995), Connolly et al. (2006), Abu-Zayyad et al. (2005)) have reported UHE CR events with energies above 10^{20} eV. The Auger array (Auger Collaboration (2004)) will soon report its results with excellent statistics.

* E-mail: G.Benford@uci.edu

† E-mail: rprother@physics.adelaide.edu.au

Meanwhile, experiments such as ANITA (Barwick et al. (2006)) and lunar Cherenkov experiments are in progress to detect the UHE neutrinos which should give clues to the origin of UHECR. See Protheroe and Clay (2004) and Falcke, Gorham & Protheroe (2004) for recent reviews of UHECR and radio techniques in UHE neutrino and particle astronomy.

Remnants of jets and their surrounding cocoons may persist long after their parent AGN fade from view. These colossal MHD structures decay slowly and yet may retain their relatively stable self-organized configurations. Decay depends on the structure circuit resistance, and lifetimes could be quite long, given the large inductance of the circuit, an initial outward current along the jet and a return current back along an outer sheath or cocoon around the jet. The current closure condition requires that a large fraction of magnetic fields resistively dissipate (Lesch et al. 1989). Also Lyutikov & Ouyed (2007) argue for direct inductive acceleration in sheared relativistic jets while the jet are on, though not afterwards. We concentrate here on the fossil era, when a substantial fraction of jet energy has already been invested in the magnetic energy of the fossil and induction occurs through decay, not in the earlier building period – though both eras can contribute to acceleration schemes.

Helical structures are common in AGN jets, arising during jet formation from rotation of magnetized plasma accreting toward the central black hole – this could be enhanced in the case of binary black hole systems. Azimuthal electric currents are therefore likely, yielding a magnetic field component along the jet direction. In radio galaxy jets boundary layers are often clearly visible in radio polarization (see, e.g. Laing & Bridle (2002) for observations and interpretation of the jets of 3C 31). Ostrowski (2002) has argued that boundary layers in jets are sites of particle acceleration.

Laboratory MHD experiments show that reversed-field pinches are fairly stable. On the immense scale of these “fossil jets”, the decay time from instability can be billions of years. However, decay of these colossal MHD structures on such time-scales result in electric fields capable of accelerating existing populations of lower energy cosmic rays up to ultra high energies with a flat spectrum extending from some minimum rigidity (momentum/charge) determined by fossil dimensions, magnetic field and decay time. We first review the properties expected of large magnetic fossils, based on extensive work in the plasma physics community over the last four decades.

2 STABILITY OF MHD STRUCTURES

We assume that the governing, evolved equilibrium of initially jet-driven, then later, long-lived magnetic structures will be a reversed field pinch (Taylor (1986), Bellan (2000)). This axisymmetric configuration has magnetic field components (in cylindrical coordinates – r, ϕ, z)

$$B_z \sim B_\phi \sim \sqrt{\mu_0 P} \quad (1)$$

in an MHD equilibrium made stable by optimally efficient radial profiles, demanding a minimum of $B_z - B_\phi$ is built by the jet current.

In a reversed-field pinch the crucial geometric feature is the longitudinal magnetic field, which changes direction at

some critical distance from the jet axis. In experiments the RFP can be curved into a torus, creating a spheromak (Bellan (2000)). We use a simple cylindrical RFP model below because, though a nearly spherical geometry may be better for an evolved fossil (especially in rich clusters with nearly isotropic pressures), the spheromak geometry imposes many field curvatures effects in particle orbits which are a complication beyond the essential physical point of the reversed axial field.

Stable, low β ($\beta = 2\mu_0 P/B^2$ where P is the plasma pressure) reversed field pinch radial profiles have several properties:

(i) B_z reverses near the outside of the confinement region. This is the crucial shear that stabilizes modes that can interchange flux tubes of plasma. It also prevents kink ($m = 1$), current-driven instabilities.

(ii) To suppress “sausage” modes driven by pressure, a value of $\beta < \frac{1}{2}$ is essential. The smaller the β , the more stabilized a confinement geometry becomes.

(iii) A conducting “wall” close enough to the plasma core to suppress the kink, $m = 1$, current-driven internal kink modes. This also completely damps all external kink modes.

(iv) A pressure profile $P(r)$ that is hollow or very flat in r , to suppress interchange of magnetic flux tubes near the magnetic axis.

Melrose, Nicholls & Broderick (1994) showed that complicated equilibrium models of an isolated, force-free magnetic flux tube could be constructed with cylindrically symmetric, force-free magnetic fields. These had a sequence of concentric layers with piecewise-constant a , where a is a running index of the equilibria in concentric cylinders, each obeying the force-free condition, $\vec{j}(r, \phi, z) = a(r)\vec{B}(r, \phi, z)$. They used analytical methods to construct models of the surface currents on these equilibria, finding some conditions such that the net current flux in the tube was zero.

For example, a “two- a model” permits current neutralization with a non-zero magnetic flux. An infinite series of equilibria are possible, yielding stable reversed-field geometries with various boundary conditions. Often a nearby conducting boundary simplifies the equilibrium as an ideal approximation.

Are such equilibria at energy equipartition between magnetic and relativistic plasma energies? Dunn & Fabian (2004) studied in cluster “ghosts” the limits on k/f , where k is the ratio of the total relativistic particle energy to that in electrons radiating between 10 MHz to 10 GHz, and f is the volume-filling factor of the relativistic plasma. Strikingly, none of their “bubbles” had a simple equipartition between the pressures from the relativistic particles and the magnetic field. Furthermore, k/f did not strongly depend on any physical parameter of the host cluster. Though at first there seemed to be two populations – k/f values around 2, another bunch around 300 – this did not hold up (Dunn, Fabian & Taylor (2005)). The apparent bimodality of the k/f distribution could be explained as arising from two kinds of jets – electron-positron, giving a low value for k , and electron-proton. If protons are the extra particles needed to maintain pressure equilibrium, but unseen in the radio emission, k is high. Also, bimodality could come from either a non-uniform magnetic field, or a filamentary structure in the lobes.

Both these possibilities are consistent with a reversed-

field equilibrium, since fields vary spatially. Variations in re-acceleration, which may occur from reconnection events in the field-reversal zone, could also affect the k/f measure. At this point we know too little to infer much. Clearly, though, constraints on the magnetic field of cluster bubbles found by comparing the synchrotron cooling time to the bubble age show that no bubbles in the sample are in equipartition.

This is plausible as laboratory experience with long-lived “magnetic bottles” such as tokomaks and reversed field pinches show that only those far from equipartition survive long. Only when the plasma pressure is far less by several orders of magnitude than magnetic field energy density do structures long persist. This is an important lesson of the applied fusion research program, now over half a century old: only low β is usefully stable.

In this spirit, we shall use the simplest possible current-neutralized, reversed-field model, with a single alpha and a nearby ideal conducting wall. It has zero total azimuthal magnetic flux since some current is carried in our assumed conducting wall. This simplification allows us to concentrate on the particle acceleration mechanisms in a simple geometry. Without this simplification, we would need a more complex equilibrium.

2.1 Evolution of Reversed-Field Magnetic Structures

Recent detections of several ghost cavities in galaxy clusters (Clarke et al. (2006)) – often, but not always, radio-emitting – suggest that the cluster hot plasma stays well separated from the bulk of the relativistic plasma on a timescale of ~ 100 Myr. Some leakage is plausible, but robust survival does occur. In cases where the radio-emitting cosmic-ray clouds are confined within the observable hot gas reservoir of the cluster, the dimensions of the X-ray hole combined with the calculated gas pressure gives a “laboratory-like” measurement of the central black hole’s energy that is converted into PdV work against the intra-cluster medium (ICM). An example is the X-ray cluster MS 0735.6+7421 observed in X-rays (Chandra) by McNamara et al. (2005) in which two large ~ 200 kpc cavities are seen in the X-ray emission; radio emission comes only from the cavities. The total energy from the AGN outburst that created these giant magnetic bubbles, and probably re-heated the cluster gas, is estimated to be $\sim 6 \times 10^{61}$ erg, of which a substantial fraction must be in magnetic field based on pressure arguments. Dynamical changes will drive inductive electric fields (Ensslin et al. (1997), Kronberg et al. (2004)). Referring to galaxy cluster embedded sources, Kronberg (2005) states that pressure balance between the magnetic field and gas (thermal and CR gas) within the holes, and the external thermal hot gas pressure implies typical B values of $\approx 20\text{--}30 \mu\text{G}$ within the holes.

So, these ghosts may be RFPs. How have they survived so long? Benford (2006) proved a theorem: that for such jet-built RFP structures, the same simple MHD stability conditions guarantee stability, even after the jet turns off. This means that magnetic structures made stable while a jet is on can evolve into fossils that persist long after the building jet current has died away. These may be the relic radio “fossils”, “ghost bubbles” or “magnetic balloons” found in clusters and made visible by contrast against the X-ray

emission as seen in Hydra A by Wise et al. (2007). Giant radio galaxies such as Cyg A are building such structures now. Such fossils have a massive inventory of magnetic energy that can be $\sim 10^{60}$ erg (Kronberg et al. (2004)). Such enormous energy can only come from the gravitational infall energy of a supermassive black hole, when jets convey a few percent of the energy outward.

These equilibria will evolve under the magnetic tension that sustains them. They are active, responsive structures, not a disordered ball of magnetic fields. In rich clusters these balloons may contract under external gas pressure. They can later rise in the gravitational potential and then expand in the lesser external pressure farther from the cluster core. Volume change will alter the plasma pressure as $p dV$ work changes the magnetic equilibrium. This in turn drives inductive electric fields, which can accelerate ions. We envision such inductive changes in response to external forces or internal evolution as the deep cause of high energy particle acceleration.

The best examples of radio bubbles are 3C 84, M87 and Her A. The edges of these bubbles are amazingly sharp, even in projection, as would be expected at the edge of a long-lived self ordered magnetic structure. Indeed, because of the helicity present in the magnetic field of the original AGN jet, the magnetic bubble it produces will retain this helicity and evolve to a self-organized force-free structure such as an RFP or sheromak, which are hard to pull apart – the toroidal field lines opposing the the lateral expansion of poloidal. The magnetic fields of these structures will therefore undergo minimal mixing with the overall cluster magnetic field, giving rise to the sharp edges seen radio images. They should thus also have larger magnetic fields than the surrounding intra-cluster medium.

Initially stable reversed field pinches become endangered by the current-driven global kink instability. This seems to be the most likely way for structures to fail when the jet current source is on, since there is more free energy to drive instability. If a structure survives the current-driven era, later stability seems more probable, as loss of the jet removes free energy. But suppose the system fails to shed magnetic helicity K as dissipation of magnetic energy proceeds (by reconnection, primarily). Such helicity loss is well known to lead to kink instability. Here we can turn to abundant laboratory experience as a guide.

2.2 The Laboratory to Astrophysical Analogy

Laboratory experiments provide much of our lore about reversed field pinches. These are all low pressure devices (low β). Taylor (1963) argued that in all systems with $\beta < 1$ magnetic reconnection conserves global magnetic helicity, allowing stable geometries to evolve without losing stability (see also Taylor (1986)). This is so even without the infinite conductivity assumption that is common in astrophysics. “Un-freezing” the magnetic field lines from plasma demands resistivity and thus some form of magnetic energy dissipation. Even so, helicity can be preserved, as in the case of dissipation by reconnection. Thus β -values approaching 1 may occur in long-lived systems if helicity (twist) may be shed through turbulent processes other than reconnection. Even if the plasma β in the jet is not small, after the jet switches off and develops into as fossil jet with a self-organized mag-

netic structure, plasma cooling and expansion is expected to lead to lower β -values. Recently, Lapenta & Kronberg (2005) have compared detailed MHD simulations with radio observations of the jet of 3C 303, a FR II with a knotty structure, with the knots appearing like self-contained magnetic structures launched along the jet. They find that in the knots $\beta \sim 10^{-5}$, and that the jet is almost certainly electromagnetically dominated rather than plasma dominated.

A magnetically driven helical dynamo can also be described as “dynamical magnetic relaxation”. Magnetic relaxation describes how structures in magnetic-pressure-dominated environments evolve to their equilibrium states. The fully relaxed state is the Taylor state, determined by minimizing the magnetic energy subject to the constraint that magnetic helicity is conserved. This leaves a force-free helical configuration with the field relaxing to the largest scale available, subject to boundary conditions. However, Taylor’s theory by itself is not a dynamical theory since it does not provide a time-dependent description of how the large scale magnetic helicity evolves.

We can draw an analogy between spheromak or reversed-field pinch formation and coronal field relaxation: the laboratory configurations form because the injection of magnetic helicity into a system takes the system away from the relaxed state. But helicity injection also drives tearing mode fluctuations that yield a finite, turbulent electromotive force. This in turn drives the system to a new relaxed state. In astrophysical coronae the situation is similar. The helical field produced by a velocity-driven dynamo inside a rotator gets buoyantly fed from below into the corona. This takes the magnetically dominated corona away from the relaxed state, but fluctuations arise, driving the system back to a relaxed state. The corona thus acts like a “laboratory” plasma volume injected with helicity from below. Injection is not at one site, but throughout the coronal-surface boundary. While each of the individual injection sites (flux tubes) is like a single laboratory configuration if the field twists get injected along the tube, each tube can also open up to even larger scales by interacting with other tubes. Magnetic energy then appears on much larger scales – a difference between the laboratory and astrophysical cases.

The dynamo effect in laboratory plasmas is a self-organization process. Resistive diffusion evolves the plasma away from a preferred state. The dynamo forces the plasma back toward the preferred, self-organized state. The resulting magnetic configuration has excess free energy leading to instabilities (or turbulence) that relax the plasma toward a state of lower magnetic energy. The plasma relaxes to the lower energy state through the “dynamo” effect. The self-generation of plasma current reconfigures the large-scale magnetic field to one with lower energy.

The structure of the relaxed state is partly captured by minimizing the magnetic energy in the plasma volume ($U_B = \int (B^2/2\mu_0)dV$) subject to the constraint of constant magnetic helicity ($K = \int \vec{A} \cdot \vec{B} dV$, where \vec{A} is the magnetic vector potential). Magnetic helicity topologically measures the knottedness of the magnetic field lines. The minimization yields a magnetic field such that the ratio of the current density to magnetic field, j/B , is a local spatial constant (the Taylor state; Taylor (1963)). For a recent comprehensive discussion of these effects, which subsumes much of the earlier

discussion especially as it unites theory and experiment, see Bellan (2000).

An experimental test of the Taylor conjecture inferred the change in magnetic energy and helicity during a relaxation event (Ji, Prager & Sarff (1995)). An approximate measurement modeled the instantaneous plasma state as a slowly varying MHD equilibrium. Since the fields during relaxation change slower than an Alfvén time, the fields satisfy the MHD force balance equation,

$$\vec{\nabla}P = \vec{j} \times \vec{B} \quad (2)$$

through discrete field twisting and braiding action. Solution of this equation with experimental constraints found that during relaxation the magnetic energy reduces by about 8%, while the magnetic helicity drops by about 3%.

The Taylor conjecture gives a useful, experimentally verified framework to depict approximately the final state of the relaxation, or dynamo, process. But it provides no information on the physical mechanism of the dynamo. Solution of the resistive nonlinear MHD equations reveals the detailed dynamics. The spatial fluctuations that underlie the dynamo are tearing instabilities driven by spatial gradients in j/B , making the field lines tear and reconnect. The MHD description of such spontaneous magnetic reconnection has been investigated for several decades. Linear theory shows that tearing instabilities grow on a timescale between a short Alfvén time (L/v_A), and the long resistive diffusion time ($\mu_0 L^2/\eta$, where η is the resistivity). For experimental plasma parameters, the theoretical growth time is approximately 100 μ s, comparable to the observed relaxation time. In astrophysical jet-built structures, this can be billions of years.

Tearing arises from a resonance between the fluctuating and mean magnetic fields. In laboratory plasma tearing occurs at many radii within the plasma, leading to large-scale reorganization. For stationary and homogeneous turbulence, magnetic helicity K is relatively conserved compared to magnetic energy during relaxation. These dynamo effects play important roles, conserving the total magnetic helicity, except for resistive effects and a small battery effect.

In astrophysical magnetic structure relaxation, charge and current imbalances adjust through the bulk, low energy plasma, which is collisional. The higher energy population can take advantage of the electric fields generated by decay, for they flow unimpeded along field lines, driven steadily by the electric fields. This is the essential picture in our model.

The turbulent dynamo effect converts magnetic helicity from the turbulent magnetic field to the mean field, when the turbulence is electromagnetic. When the turbulence is electrostatic or due to the electron diamagnetic effect, the magnetic helicity of the mean magnetic field gets transported across space. Two types of electric fields get generated during reconnection in the RFP. One is the helical electric field accompanying the helical tearing mode that causes the reconnection. The second is a mean, or axisymmetric, electric field induced by the flux change driven by the tearing mode dynamo. Clearly this is a complicated phenomenon.

We do not attempt to treat such details. Instead, we shall simply take the inductive electric fields to be a fraction of the mean magnetic field. In the absence of detailed knowledge of the structure, this seems a good way to begin.

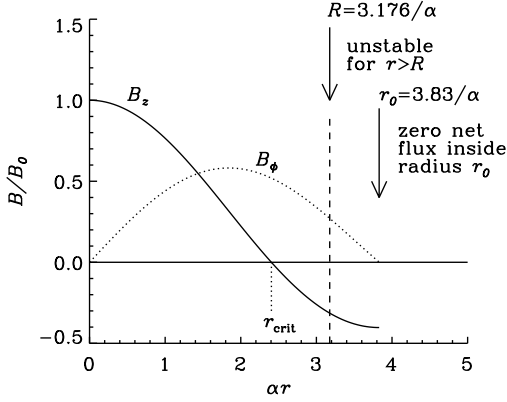


Figure 1. Magnetic field components of an RFP.

2.3 Properties of a simple reversed field pinch

The simplest idealization would be for an infinite cylindrical jet where the magnetic field in cylindrical coordinates (r, ϕ, z) is (Lundquist (1951))

$$B_r = 0, \quad B_\phi(r) = B_0 J_1(\alpha r), \quad B_z(r) = B_0 J_0(\alpha r), \quad (3)$$

and this has been shown (Voslamber & Callebaut (1962)) to be stable for $\alpha r < 3.176$. This radius for stability which we take to be $R = 3.176/\alpha$ is where a conducting wall with a large inertial mass would be present in an experimental situation, and provide part of the circuit along which a return current could flow, which we assume here to be the cocoon. The magnetic field is shown in Fig. 1. Notice the longitudinal field changes sign at $r_{\text{crit}} = 2.405/\alpha$, the first zero of $J_0(\alpha r)$.

One can use Ampère's law to find the current density

$$\vec{j}(r) = \frac{1}{\mu_0} (\vec{\nabla} \times \vec{B}) = \frac{\vec{B}(r)\alpha}{\mu_0} \quad (\text{A m}^{-2}), \quad (4)$$

which is everywhere proportional to the magnetic field. From this, the vector potential is

$$\vec{A}(r, \phi, z) = \frac{1}{\alpha} \vec{B}(r, \phi, z). \quad (5)$$

The outward electric current (positive j_z) is associated with radii $r < r_{\text{crit}}$ and the return current with radii $r > r_{\text{crit}}$,

$$I_{\text{out}} \approx (1.8 \times 10^{18} \text{ A}) \times \left(\frac{B_0}{3 \mu\text{G}} \right) \left(\frac{R}{100 \text{ kpc}} \right), \quad (6)$$

$$I_{\text{ret}} \approx (5 \times 10^{17} \text{ A}) \times \left(\frac{B_0}{3 \mu\text{G}} \right) \left(\frac{R}{100 \text{ kpc}} \right) \quad (7)$$

and so some of the return current must be at radii $r > R$ — in the outer part of the cocoon or in the interstellar medium of the host galaxy in order to exactly balance the outward current.

The plasma pressure may be calculated from Eq. 1 of Robinson (1971), i.e.

$$\frac{dP}{dr} + B_z \frac{dB_z}{dr} + \frac{B_\phi}{r} \frac{d}{dr} (r B_\phi) = 0. \quad (8)$$

Solving this for \vec{B} given by Eq. 3 results in $P = \text{constant}$. That is, for \vec{B} given by Eq. 3 the tension of the azimuthal field lines perfectly balances the radially outward pressure of the longitudinal field.

3 CHARGED PARTICLE MOTION AND ACCELERATION

The critical radius, r_{crit} , where the longitudinal field B_z changes sign, is also the radius where the longitudinal current density j_z changes sign. It is also here that reconnection may occur and may be a site of particle acceleration. Lesch, Birk & Schopper (2002) have considered acceleration in AGN jets due to a reconnection electric field *along* the length of the jet of an active quasar. That paper shows acceleration of hadrons to UHE should be possible in active AGN jets. The *length* of the jet is critical in their model, determining the maximum energy. We differ in that the reconnection electric field is azimuthal, i.e. *around* the fossil cylinder. Also, there should be many nearby remnants, so they can accelerate UHECRs, whereas active quasars tend to be at high redshift, and so their UHECRs will suffer the GZK cutoff if they are more than ~ 10 Mpc away.

3.1 Energy of Reconnection: Plasma Wave Model

Rather than assign a fixed fraction of the ambient magnetic field energy to the generated reconnection electric field, we can use results from laboratory observations in reversed field pinches (Ji et al. (2004); Ji, Prager & Sarff (1995)). The zone where B_z reverses will probably be the reconnection site, since there only the azimuthal field needs to reconnect.

In reconnection regions, micro-instabilities enhance resistivity, driving the reconnection rate. These arise from both electromagnetic and electrostatic modes. The electrostatic lower hybrid drift instability has been invoked, but recent work shows that it does not occur in the high- β regions where reconnection occurs. There, electromagnetic instabilities prevail, as the B_z field moves radially toward the reconnection region, in our assumed cylindrical geometry, preferentially annihilating in the zone where B_z reverses sign. This drives an azimuthal electric field. The plasma is highly collisionless, so the induced resistivity greatly exceeds the Spitzer level. The cause of this is ultimately the enhanced modes, such as the modified two-stream instability, which in experiment appear localized in the high-beta region where reconnection occurs. Magnetic fluctuations B_1 appear also, correlated strongly with resistivity enhancement (Ji et al. (2004)).

We can estimate the equivalent electric field generated in reconnection by noting that a momentum p per unit volume appears in the electromagnetic waves,

$$p/V = \frac{k \langle B_1^2 \rangle}{\omega \mu_0} \quad (9)$$

Momentum moves from background plasma electrons and ions to the electromagnetic fluctuations at a rate 2γ , where γ is the nonlinear damping rate on the electron-ion background plasma. In this highly nonlinear state, experiments show that $\gamma \sim \omega$, the unstable mode frequency. Loss of momentum is a force equivalent to an effective electric field in the reconnection region, E_{rec} , given by

$$enE_{\text{rec}} = 2k\gamma \frac{\langle B_1^2 \rangle}{\omega \mu_0} \quad (10)$$

The magnetic wave fluctuation levels seen in experiment are of magnitude $B_1 \sim 0.05$ the ambient averaged

inflow field levels, B_z . We thus set $B_1 = gB_z$ and the fraction $g = 0.05$. Further, from experiment the observed wavelengths of this turbulence are the size of the coherence lengths in the fields, strongly suggesting a cooperative role (Ji et al. (2004)). The relevant wavenumber k is the inverse Larmor radius of background electrons in the plasma,

$$r_L = (10 \text{ m}) \times (T_{\text{eV}})^{-1/2} \left(\frac{B_0}{\mu\text{G}} \right)^{-1} \quad (11)$$

(Ji et al. (2004)).

Scaling the results of laboratory experiments, we find

$$E_{\text{rec}} = (1.5 \times 10^{-6} \text{ V m}^{-1}) \times \left(\frac{g}{0.05} \right)^2 \times \left(\frac{B_z}{10 \mu\text{G}} \right)^3 (T_{\text{keV}})^{1/2} \left(\frac{n}{10^6 \text{ m}^{-3}} \right)^{-1} \quad (12)$$

with n being the plasma density, and taking $B_z \sim 10 \mu\text{G}$ and assuming the heated region has keV energies. To attain fields of order 10^{-4} V/m then requires g a bit larger, and perhaps B of $100 \mu\text{G}$. Plasma temperature may also be higher than keV, and density lower, also increasing E_{rec} . These parameter ranges would yield 10^{20} eV protons after several encounters with such structures of scale $\sim \text{Mpc}$. Thus, we consider the possibility of UHE CR getting sequential boosts in energy as a result of multiple encounters with different fossils in a similar way that Ip & Axford (1992) envisage Galactic cosmic rays get re-energized by multiple interactions with supernova remnants in the Galactic disk.

We expect it to be realistic to assume that electric fields outside the reconnection zone can also accelerate particles. The cold plasma (pressure is low) responsible for currents which maintain the magnetic structure cannot short out these electric fields, since they are inductively driven everywhere in the structure, allowing acceleration outside the reconnection zone. Next we investigate whether or not this alone will be viable for accelerating UHECR. In what follows we assume that electric fields outside the reconnection zone can accelerate particles.

3.2 Global Electric Fields from RFP Decay

Electric fields from reconnection are *emfs* induced according to Faraday's law, and so the electric field will be more extensive. Assuming a flow of flux lines toward the reconnection region, the field will be changing everywhere and will induce an electric field. The simplest way of estimating this global reconnection electric field is by assuming an exponential decay of the magnetic field,

$$\vec{B}(t) = B_0 e^{-t/t_{\text{dec}}} [J_1(\alpha r) \hat{\phi} + J_0(\alpha r) \hat{z}]. \quad (13)$$

Then,

$$\vec{E} = -\frac{\partial \vec{A}}{\partial t} = \frac{\vec{B}}{t_{\text{dec}} \alpha}, \quad (14)$$

$$\vec{E} \approx 3.18 \times 10^{-5} \left(\frac{B_0}{10 \mu\text{G}} \right) \left(\frac{R}{100 \text{ kpc}} \right) \left(\frac{t_{\text{dec}}}{\text{Gyr}} \right)^{-1} \times [J_1(\alpha r) \hat{\phi} + J_0(\alpha r) \hat{z}] e^{-t/t_{\text{dec}}} \quad (\text{V/m}) \quad (15)$$

The rate of change of the particle momentum $p = \beta\gamma mc$

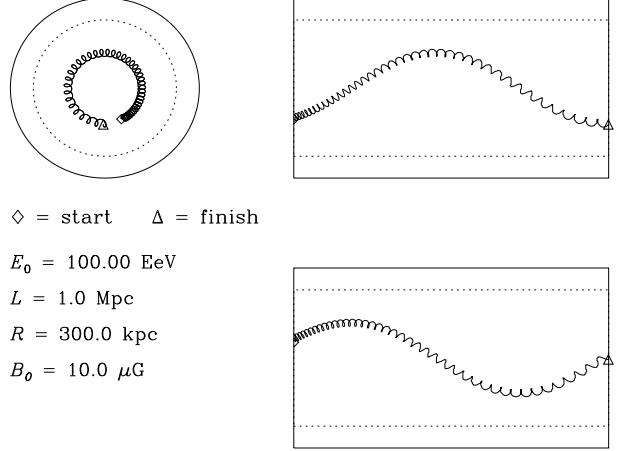


Figure 2. Three orthogonal views showing a typical orbit in the RFP fields, and critical radius (dashed).

(neglecting losses) of a relativistic charge Ze is then

$$\frac{d\vec{p}}{dt} = ZecB(\vec{\beta} \times \hat{B} + \beta_{\text{dec}} \hat{B}), \quad \text{where } \beta_{\text{dec}} = \frac{R}{ct_{\text{dec}}}, \quad (16)$$

such that a simple 1st order integration scheme might be

$$\vec{r}(t + \Delta t) = \vec{r}(t) + c\Delta t \vec{\beta}(t), \quad (17)$$

$$\vec{p}(t + \Delta t) = \vec{p}(t) + \frac{c\Delta t}{r_{\text{gyro}}(\vec{r})} p \times [\vec{\beta}(t) \times \hat{B}(\vec{r}) + \beta_{\text{dec}} \hat{B}(\vec{r})], \quad (18)$$

$$\text{where } r_{\text{gyro}}(\vec{r}) = \frac{\gamma\beta mc}{ZeB(\vec{r})}. \quad (19)$$

Using this scheme we have conducted simulations of charged particle motion in the RFP magnetic field including the effect of energy change in the induced electric field. We inject particles uniformly and isotropically over the surfaces of disks of radius R at both ends of the jet, and follow their motion until they escape. A typical example is shown in Fig. 2.

Ultra-relativistic particles of charge Ze are injected with energy E_0 (note for ultra-relativistic particles $E \approx pc$) and their final energies are binned as shown in Fig. 3. Since the induced electric field is in the same direction as the magnetic field, energy is gained as particle move *along* field lines. Thus we have also carried out simulations in which the particle's position is simply advanced along a field line, gaining momentum $ZeE\Delta t$ in step $c\Delta t$. Results for this case with high statistics (solid curves) are in agreement with the results for full gyro motion. We have shown that for a decaying RFP, in which the electric field is everywhere parallel to the magnetic field, cosmic ray nuclei will gain energy unimpeded except by pion photoproduction on the CMBR – as they undergo helical motion around magnetic field lines their momentum component parallel to \vec{B} increases, while their momentum component perpendicular to \vec{B} and the gyroradius remains constant, as is seen in the trajectory shown in Fig. 2. Note that the “double peaked” structure (Fig. 3) is due to separate contributions from injection at $r < r_{\text{crit}}$ and $r > r_{\text{crit}}$, as we shall show in the next section.

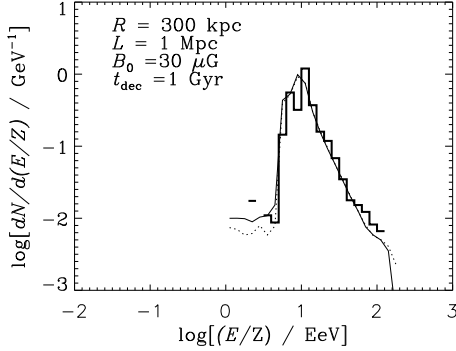


Figure 3. Example output spectra (histograms) for monoenergetic injection at $p_0c/Z = 10^{18}$ eV, and fossil jet parameters as specified and following particle trajectories as they undergo helical motion along field lines. Solid curve shows results for case of neglecting gyromotion and simply following the gyrocentre motion, and dashed curve shows effect of neglecting time dependence of field (valid provided $t_{\max} \ll t_{\text{dec}}$).

3.3 Analytic approach

No approximations were made in obtaining the energy spectrum, shown as the histogram in Fig. 3, by following particle trajectories in the electromagnetic field of a decaying RFP. To obtain an approximate analytic result, we can assume that a particle follows a helical path with its guiding centre on a single field line from one end of the jet to the other. Since the induced electric field is proportional to the magnetic field according to Eq. 15, positively charged particles will gain energy for pitch angles less than 90° and lose energy if their pitch angles are greater than 90° .

The energy gain on traversing the jet length L will actually depend on the pitch angle ψ of the helical magnetic field line acting as the guiding centre. So, positive particles injected into the RFP with $r < r_{\text{crit}}$ will gain energy while moving in the positive z direction, and those injected with $r_{\text{crit}} < r < R$ will gain energy while moving in the negative z direction. The increase in momentum of ultra-relativistic particles of charge Ze is

$$p_{\text{gain}} = \frac{ZeEL}{c \cos \psi} \quad (20)$$

where

$$\vec{E} = \frac{\vec{B}}{t_{\text{dec}}\alpha} = B_0 \frac{J_1(\alpha r)\hat{\phi} + J_0(\alpha r)\hat{z}}{t_{\text{dec}}\alpha}, \quad (21)$$

$$\cos \psi = \frac{B_z}{B} \quad (22)$$

Hence,

$$p_{\text{gain}}c = \frac{ZeL}{t_{\text{dec}}\alpha} \frac{B^2}{B_z} = \frac{ZeB_0L}{ct_{\text{dec}}\alpha} \frac{J_0(\alpha r)^2 + J_1(\alpha r)^2}{J_0(\alpha r)}, \quad (23)$$

$$E_{\text{gain}} = E_{\text{gain}}^0 \frac{J_0(\alpha r)^2 + J_1(\alpha r)^2}{J_0(\alpha r)} \quad (24)$$

where

$$E_{\text{gain}}^0 \approx (10^{18} Z \text{ eV}) \left(\frac{B_0}{10 \mu\text{G}} \right) \left(\frac{L}{\text{Mpc}} \right) \times$$

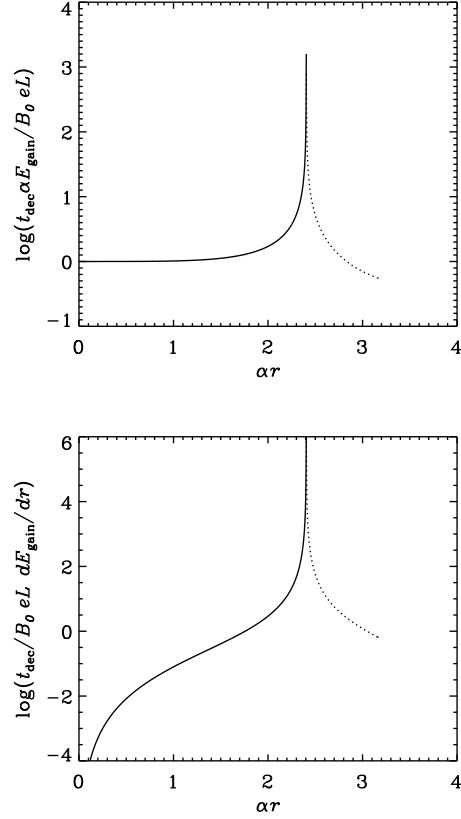


Figure 4. (a) Momentum gain of particles injected at one end of the RFP of length L and exiting at the other. Solid curve for positive particles traveling in positive z direction, dotted for positive particles traveling in negative z direction. (b) The function dp_{gain}/dr

$$\times \left(\frac{R}{100 \text{ kpc}} \right) \left(\frac{t_{\text{dec}}}{\text{Gyr}} \right)^{-1} \quad (25)$$

and this is plotted in Fig. 4(a). Note that as $r \rightarrow r_{\text{crit}}$, $p_{\text{gain}} \rightarrow \infty$.

We can work out the energy spectrum as follows,

$$\frac{dN}{dE_{\text{gain}}} = \frac{dN}{dp_{\text{gain}}c} = \frac{dN}{dr} \left[\frac{dp_{\text{gain}}c}{dr} \right]^{-1} \quad (26)$$

where dN/dr is the distribution in radius of the injection points. For injection at one end of the RFP we would have uniform injection over the disk of radius R , giving

$$\frac{dN}{dr} = \frac{2r}{R^2} \text{ for } 0 < r < R. \quad (27)$$

Differentiating Eq. 23 gives

$$\frac{dp_{\text{gain}}c}{dr} = \frac{ZeB_0L}{t_{\text{dec}}} \left[\frac{J_1(\alpha r)J_0(\alpha r)^2 - J_0(\alpha r)J_1(\alpha r)J_2(\alpha r)}{J_0(\alpha r)^2} \right] \quad (28)$$

which is plotted in Fig. 4(b).

Thus, from Eqn. 26 we have dN/dp_{gain} as a function of the parameter r , and from Eqn. 24 we have p_{gain} as a function of the parameter r , and so we can plot dN/dp_{gain} vs. p_{gain} , and this is shown in in Fig. 5. In Fig. 6 we compare the analytical spectrum with that obtained by following particle orbits. This analytic slope, which asymptotically is E^{-2} , is

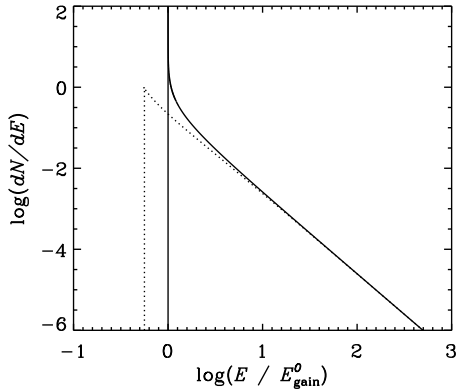


Figure 5. Spectrum of accelerated particles. (Curves have same meaning as in Fig. 4)

consistent with that of Fig. 5. The agreement reflects a geometric property of the acceleration mechanism, as particles near the reconnection region experience little axial magnetic field. By our simplifying assumption that the inductive electric field is proportional to the equilibrium magnetic field, we find that such particles near the reconnection site then are accelerated around the axis by the purely azimuthal electric field. This generally keeps them in the structure longer, as they do not move radially very much, so they leave only when they have drifted down the axis to the end. Those which enter the fossil near the reconnection zone will be preferentially accelerated, becoming UHECRs. This gives a clean mapping of geometry into the energy spectrum. Such spectra yield 10^{20} eV protons and iron nuclei 26 times more energetic. Repeated accelerations in random fossils along a particle route could maintain this quality if fossils are common enough, and have sufficient decaying energy, in our region of the universe.

Finally, Heinz & Sunyaev (2002) have shown that particles should be accelerated at the reverse shock of a micro-quasar jet colliding with the interstellar medium, and that this may give a contribution to the galactic cosmic rays up to about ~ 10 GeV. Here, we consider the possibility of particle acceleration by electric fields in fossil micro-quasars induced by the decay of a remnant magnetic bubble after the jets have switched off, as in the case of fossil AGN. This mechanism might work for and pulsar wind nebulae as well as fossil micro-quasars, and be responsible for emission in unidentified TeV sources, as well as contributing to galactic CR. In either case the expected minimum energy would be

$$E_{\text{gain}}^0 = (10^{12} Z \text{ eV}) \left(\frac{B_0}{0.1 \text{ mG}} \right) \left(\frac{L}{1 \text{ pc}} \right) \times \left(\frac{R}{1 \text{ pc}} \right) \left(\frac{t_{\text{dec}}}{\text{Myr}} \right)^{-1}. \quad (29)$$

4 DISCUSSION

Active galaxies have long been considered as a source of the UHE CR, for example Rachen & Biermann (1993) considered acceleration at shocks associated with hot spots in

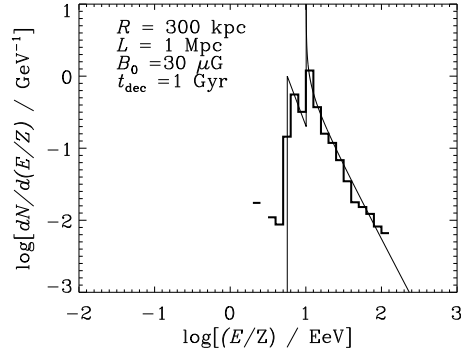


Figure 6. Example output spectra (histograms) for monoenergetic injection at $p_0 c/Z = 10^{18}$ eV, and fossil jet parameters as specified and following particle trajectories as they undergo helical motion along field lines. Solid curve shows analytic result.

lobes of Fanaroff-Riley II (FR II) radio galaxies. There is no simple connection between the maximum particle energy attainable in an AGN jet, in the hot spot, and in the subsequent bubble. In the case of a jet, either the magnetic field through proton synchrotron radiation or pion photoproduction interactions will stop the acceleration process (Mücke & Protheroe (2001)), whereas in the case of hot spots in lobes of FR IIs the dimensions of the shock, its speed and magnetic field configuration would determine the maximum energy. Ultimately, pion photoproduction on the CMBR cannot be avoided, and for shock acceleration with plausible parameters it is difficult to exceed $\sim 10^{21}$ eV (Protheroe (2004)). In the case FR II jets (or quasar jets) pion photoproduction on the photon field of a luminous accretion disk will cut off the spectrum of accelerated protons well below this. However, in the case of FR I jets (or the jets of BL Lac objects), having under-luminous disks or advection dominated accretion flows, the cut-off will be due to synchrotron losses or pion photoproduction on the jet synchrotron photons. The problem of escape of the highest energy protons trapped by a jet's magnetic field can be solved by the same photoproduction interactions, which convert protons to neutrons which escape before decaying, and if travelling in the jet direction the resulting cosmic ray protons have higher energies from Doppler boosting (see Protheroe et al. (2003) for the case of M87).

Once accelerated to the ultra-high energy region, protons can more readily escape their birth fossil. They will move through the tens of Mpc where the GZK photo-pion scattering from the background microwave radiation begins to take its toll. As well, the UHECRs will scatter from other fossils. This can make them appear isotropic if their directions are scattered enough, and they can be further accelerated by these other fossils as well.

Our model is geometrically simple, to capture the essential geometry of reverse field pinches, and the acceleration physics that affords to particles, depending on where they are in the structure. We have neglected important effects:

(i) Scattering – this in principle will rearrange particle orbits, moving some out of the high-acceleration zone by

scattering their pitch angles, but also scattering others into the preferential region. In the highly ordered field of AGN fossils, this may be less important for energization to UHE of a pre-existing population of high energy cosmic rays accelerated, e.g. in the host galaxy of the dead AGN. Future work should nevertheless include investigation of scattering of lower energy particles by the magnetic turbulence expected in such sources, generated by the inductive effects of their slow collapse and by the ongoing reconnection events near the axial field reversal sites.

(ii) Energy losses - here we have neglected energy losses by, e.g. pion photoproduction and adiabatic expansion. For the range of model parameters used in the present work, these occur more slowly than acceleration, but should be included in future work.

(iii) Geometry. Assuming a cylindrical reversed field pinch omits the many possible curvatures a more spherical RFP i.e., a spheromak would entail. External pressure will not be isotropic, generally. But if a fossil becomes detached from its parent galaxy presumably by reconnection of fields at the feet of the former jet structure it can rise, buoyant, in any cluster gas. The shape will resemble a fat torus, with the currents forming loops. We simplified this, feeling that torodial curvature would complicate our calculations without adding new physics. This can be relaxed in future, using more complicated equilibria.

(iv) Initial energy. To isolate the highest energy particle issues, we began with a population of constant energy particles, e.g. 1 EeV, but provided the injection energies are much less than the minimum energy gained, by particles being accelerated along the fossil jet, axis the final spectral shape is insensitive to the initial energy. Generalizing to an initial energy spectrum will be done in future. This said, we have produced spectra that yield very high energy particles. 10^{20} eV protons and iron nuclei 26 times more energetic still. If 1% of the universe is taken up with fossils (Kronberg (1994)), of size < 1 Mpc, then there should be many fossils within 100 Mpc of us. A fresh structure is under construction at M87, 16 Mpc away. This leads us to predict that while Auger should see a smooth UHECR background above the GZK cutoff, $\sim 6 \times 10^{19}$ eV. Auger may see clumps of UHECR in the sky, which point back to nothing specially luminous. These will be fossils we didn't know about—plus some we did. The UHECR will then become a diagnostic of regions storing vast magnetic energies, yet perceptible only through equally energetic particles, bringing word of them across great distances.

The total energy stored in the magnetic field of an RFP is

$$U_B = 1.3 \times 10^{59} \left(\frac{B_0}{10 \mu\text{G}} \right)^2 \times \left(\frac{L}{\text{Mpc}} \right) \left(\frac{R}{100 \text{ kpc}} \right)^2 \text{ (erg)}. \quad (30)$$

These magnetic structures must have survived since the quasar was last active, implying a decay time scale t_{dec} of the order of Gyr, so

$$\dot{U}_B = \frac{U_B}{t_{\text{dec}}}, \quad (31)$$

$$\dot{U}_B = (4.0 \times 10^{42} \text{ erg s}^{-1}) \times \left(\frac{B_0}{10 \mu\text{G}} \right)^2 \times \left(\frac{L}{1 \text{ Mpc}} \right) \left(\frac{R}{100 \text{ kpc}} \right)^2 \left(\frac{t_{\text{dec}}}{\text{Gyr}} \right)^{-1}. \quad (32)$$

assuming that the reconnection is continuous and uniform along the cylindrical reconnection region, such that the whole magnetic structure slowly decays exponentially on time scale t_{dec} while maintaining the stable configuration given by Eq. 3.

O'Neill et al. (2006) have examined the interactions of AGN jets with magnetized cluster media using MHD jet simulations in a cluster-like atmosphere extending over distances ~ 200 kpc. They find that steady jets asymptotically deposit $\sim 50\%$ of their power into ambient thermal energy, $\sim 25\%$ into heating of the ICM, and the remaining energy to be mostly stored in the jet backflow cocoon, and that magnetic energy introduced by the jet is generally amplified, especially by sheared flows; see also Ryu et al. (1998).

For an extragalactic source distribution locally producing an E^{-2} spectrum of protons, Lipari (2005) estimates the local power requirement to be $\sim 10^{50}$ erg Mpc $^{-3}$ y $^{-1}$. Decaying magnetic fields with local filling factor η_B lose energy at a rate

$$\dot{u}_B \sim 10^{53} \eta_B \left(\frac{B_0}{10 \mu\text{G}} \right)^2 \left(\frac{t_{\text{dec}}}{\text{Gyr}} \right)^{-1} \text{ erg Mpc}^{-3} \text{ y}^{-1}$$

Magnetic fields from quasars can fill up to 5–20% of the intergalactic medium (Furlanetto & Loeb (2001)) – probably higher locally since our Galaxy is in a “Wall”. Indeed, Gopal-Krishna & Wiita (2001) estimate the fractional relevant volume that radio lobes born during the quasar era cumulatively cover is ~ 0.5 . Hence our crude energetics arguments show fossil AGN structure decay could well be responsible for the observed UHE CR.

The spectrum of accelerated particles will cut off at some maximum momentum determined by either the finite thickness of the reconnection zone (recall that in the analytic approximation as $r \rightarrow r_{\text{crit}}$, $p_{\text{gain}} \rightarrow \infty$), or by the gyroradius increasing so that it is no longer much less than the radius of the fossil. From Fig. 1, we see that for $r < R$ the magnetic field is in the range $0.4B_0 < B < B_0$. Hence, the condition $r_L \ll R$ implies

$$E_{\text{gain}}^{\text{max}} \ll (10^{21} \text{ Z eV}) \left(\frac{B_0}{10 \mu\text{G}} \right) \left(\frac{R}{100 \text{ kpc}} \right). \quad (33)$$

The UHECR spectrum shows a steepening just below 10^{18} eV (the “dip”) followed by a flattening at around 10^{19} eV (the “ankle”) before the possible observed GZK cut-off just above 10^{20} eV. Berezhinsky et al. (2006) favour a scenario in which extragalactic cosmic rays are injected with an $E^{-2.7}$ spectrum above $\sim 2 \times 10^{18}$ eV, and show that the observed spectral feature referred to as the “dip” could then be due to to Bethe-Heitler pair production on the CMBR. While their model fits are impressive, we believe that models in which the galactic cosmic rays extend up to a few 10^{18} eV and have extragalactic cosmic rays injected with an E^{-2} spectrum, or similar, e.g. following diffusive shock acceleration at Fanaroff-Riley Class II radio galaxy hot-spots (Rachen & Biermann 1993), are by no means ruled out. Indeed, Hillas (2006) has shown that by adding galactic and

extragalactic spectra with various power-law source spectra and compositions several possibilities, including source spectra with an $E^{-2.2}$ spectrum, are consistent with the data. While a single ideal cylindrical RFP with particle injection over its ends yields an E^{-2} spectrum, the spectrum due to several with different maximum energies would inevitably be steeper. Very recent results from the Pierre Auger Observatory (Yamamoto et al. 2007) are not yet conclusive, but appear to be consistent with source spectral index in the range 2.2–2.5.

The spectrum of UHECR observed at Earth would have contributions from nearby fossil jets at different distances, with different powers and each having different dimensions and magnetic fields, and hence a range of E_{gain}^0 and $E_{\text{gain}}^{\text{max}}$. For an individual fossil, the cut-off is expected to be rigidity dependent, implying the observed composition would change from light to heavy close to the cut-off if one or two nearby AGN fossils dominate. However, if distant sources dominate nuclei will be photo-disintegrated by interactions with CMBR photons, and in this case the composition would remain light to the highest energies if distant sources or fossils dominated. Otherwise the composition could be mixed near the observed cut off.

Nearby potential sources of UHE CR would include the bubbles around Cen A, the nearest powerful radio galaxy, and around M87. Radio observations at 20 cm of Cen A by Morganti et al. (1999) indicate the presence of large features, one of which has been interpreted by Saxton et al. (2001) as a buoyant bubble of plasma deposited by an intermittently active jet. Even closer, in M87 there are two bubbles of synchrotron emission which appear to be inflated by outflows from the central engine visible in the low frequency radio data of Owen et al. (2000), with an amazingly sharp edge indicating the possible presence of a shock. Given the very high mass of the central black hole in M87, its jet, although fairly powerful, is weak compared to its Eddington limit, making M87's bubbles a prime candidate as a UHE CR accelerator.

As we expect most of the fossil jets to be below the sensitivity of current radio telescopes, it is impossible at the present time to make firm predictions for the expected UHECR intensity at Earth. A low synchrotron surface brightness, only observable if at all at low frequency, does not necessarily mean that the magnetic field is low. Rather, we would argue that it is the cooling of the relativistic electrons by synchrotron emission, since the last AGN outburst which filled the bubble, that has reduced the synchrotron emissivity. However, such fossils may well be observable when the SKA (<http://www.skatelescope.org/>) is commissioned, hopefully within ~ 10 years. Nevertheless, we have demonstrated that it is possible for this process to accelerate protons to UHE, and nuclei to a Z times higher energy, and shown that the power requirements may reasonably be achieved given plausible volume filling factors.

Very recent anisotropy data from the Pierre Auger Observatory (Armengaud et al. (2007), Harari et al. (2007)) show no significant large-scale anisotropy or correlation of cosmic ray arrival directions with BL Lac objects. Perhaps this is not surprising because propagation of cosmic rays through intergalactic magnetic fields will tend to isotropize their arrival directions, except perhaps for UHE CR protons at the highest energies from very nearby extragalactic

sources. With longer exposure times Auger may see such anisotropies, in which case the most probable source candidates would be bubbles around Cen A and M87. Neutrino observatories may, in principle, see UHE neutrinos originating from directions close to UHE cosmic ray acceleration sites, through pion photoproduction interactions of the UHE CR on the CMBR during propagation from their sources. These “GZK neutrinos” would appear as haloes around the true source direction. Of course, if such haloes appear where there are no obvious source candidates, they could well be from fossil jets with very low surface radio brightness.

Future work will include exploring observational consequences of this model at radio, X-ray and gamma-ray energies. Will electron acceleration (in opposite direction to protons) be killed by streaming instability, or by other processes? If so, this will heat the plasma. Could this be seen in X-rays? If not, radio synchrotron and gamma-ray signals could be generated. Could these be detectable by existing radio telescopes or by the SKA in coming decades, or by GLAST (<http://glast.stanford.edu/>)? How much of the energy of a fossil AGN goes into cosmic rays? Finally, we mention the possibility that this mechanism operating for microquasars might be responsible for acceleration of some of the Galactic population of cosmic rays.

In conclusion, remnants of jets and their surrounding cocoons may still be present around or close to galaxies which contain AGN which are now no longer active. These fossil jets are colossal MHD structures and may have total energies $\sim 10^{60}$ erg. After a jet switches off, the fossil jet will organize itself into a stable configuration, such as the reverse-field pinch in which the longitudinal magnetic field changes direction at a critical distance from the axis, leading to re-connection there, and to slow decay of the large-scale RFP field. We have shown that this field decay induces large-scale electric fields which accelerate cosmic rays an E^{-2} power-law up to ultra-high energies. Energetics arguments show that this provides a plausible mechanism for the origin of the UHE CR.

ACKNOWLEDGENTS

We thank Garang Yodh and Roger Blandford for stimulating discussions, and KIPAC and SLAC for hospitality in May 2007. We also thank the anonymous referee for helpful comments. RJP thanks the Australian Research Council for support through a Discovery Project.

REFERENCES

- Abu-Zayyad T. et al., 2005, *Astropart. Phys.*, 23, 157
- Armengaud E., for the Pierre Auger Collaboration, 2007, 30th International Cosmic Ray Conference, Merida Mexico, July 2007, in press. arXiv:0706.2640v1 [astro-ph]
- Auger Collaboration, 2004, *NIM*, 523, 50
- Barwick S.W. et al., 2006, *Phys. Rev. Lett.*, 96, 171101
- Bellan P., 2000, “Sphereomaks”, Imperial College Press
- Benford G, 2006, *Mon. Not. R. Astron. Soc.* 369, 77
- Berezinsky V., Gazizov A., & Grigorieva S., 2006, *Phs. Rev. D*, 74, 043005
- Bird D.J. et al., 1995, *ApJ*, 441, 144

- T. Clarke, E. Blanton, C. Sarazin, N. Kassim, L. Anderson, H. Schmitt, Gopal-Krishna, D. Neumann, To appear in the Proceedings of "Heating vs. Cooling in Galaxies and Clusters of Galaxies", eds. H. Boehringer, P. Schuecker, G. W. Pratt & A. Finoguenov (ESO Astrophysics Symposia, Springer-Verlag), Garching (Germany), August 2006, ArXiv Astrophysics e-prints, arXiv:astro-ph/0612595
- Connolly B.M., BenZvi S.Y., Finley C.B., O'Neill A.C., Westerhoff S., 2006, Phys.Rev., D74, 043001
- Dunn R.J.H., Fabian A.C., 2004, MNRAS, 351, 862
- Dunn R.H., Fabian A.C., and Taylor G.B., 2005, MNRAS 364, 1343
- Ensslin T.A., Biermann P.L., Kronberg P.P., Wu X.- P., 1997, ApJ 477, 560
- Ensslin T.A., 2003, A&A, 401, 499
- Falcke H., Gorham P., Protheroe R.J., 2004, New Astron. Rev., 48, 1487
- Freidberg, Jeffrey P., 1987, "Ideal Magnetohydrodynamics", Plenum Press, New York
- Furlanetto S.R., & Loeb, A., 2001, ApJ, 556, 619
- Gopal-Krishna, & Wiita P. J., 2001, ApJL, 560, L115
- Greisen K., 1966, Phys. Rev. Letters, 16, 748
- Harari D, for the Pierre Auger Collaboration, 2007, 30th International Cosmic Ray Conference, Merida Mexico, July 2007, in press. arXiv:0706.1715v1 [astro-ph]
- Heinz S., & Sunyaev R., 2002, Astron.Astroph., 390, 751
- Hillas A. M., 2006, ArXiv Astrophysics e-prints, arXiv:astro-ph/0607109
- Ip W.-H., & Axford W. I., 1992, Particle Acceleration in Cosmic Plasmas, 264, 400
- Ji, H., Terry, S., Yamada, M., Kuhsrud R., Kuritsyn A., & Ren Y., 2004, Physical Review Letters, 92, 115001
- Ji H., Prager S. C., & Sarff J. S., 1995, Physical Review Letters, 74, 2945
- Kronberg P.P., Colgate S.A., Li H., & Dufton Q.W., 2004, ApJL, 604, L77
- Kronberg P.P., 2005, Magnetic Fields in Galaxy Systems, Clusters and Beyond, Lect. Notes Phys., 664, 9
- Kronberg P.P., 1994, Rep. Prog. Phys. 57, 325
- Laing R. A., & Bridle A. H. 2002, MNRAS, 336, 328
- Lapenta G., & Kronberg P.P., 2005, ApJ, 625, 37
- Lesch H., & Birk G.T., 1998, ApJ, 499, 167
- Lesch H., Birk G.T. & Schopper R., 2002, Plasma Physics & Controlled Fusion, 44, B1
- Lesch H., Appl S., & Camenzind, M. 1989, Astron.Astroph., 225, 341
- Lyutikov M., & Ouyed, R. 2007, Astroparticle Physics, 27, 473
- Lipari P., 29th International Cosmic Ray Conference, Pune, vol. 6, 381, 2005
- Lundquist S., 1951, Phys. Rev., 83, 30
- Melrose D.B., Nicholls J. and Broderick N.B., 1994, J. Plasma Phys, 51, 163
- Morganti R., Killeen N. E. B., Ekers R. D., & Oosterloo T. A., 1999, MNRAS, 307, 750
- Mücke A., & Protheroe R. J., 2001, Astroparticle Physics, 15, 121
- O'Neill S. M., Jones T. W., Tregillis I. L., & Ryu D., 2006, Astronomische Nachrichten, 327, 535
- Ostrowski M., 2002, Memorie della Societa Astronomica Italiana, 73, 387
- Owen F. N., Eilek J. A., & Kassim N. E., 2000, ApJ, 543, 611
- Protheroe R. J., Donea A.-C., & Reimer A., 2003, Astroparticle Physics, 19, 559
- Protheroe R. J., 2004, Astroparticle Physics, 21, 415
- Protheroe R.J. and Clay R.W., 2004, PASA, 21, 1
- Rachen J. P., & Biermann P. L., 1993, Astron.Astroph, 272, 161
- McNamara B. R., Nulsen P. E. J., Wise M. W., Rafferty D. A., Carilli C., Sarazin C. L., & Blanton E. L., 2005, Nature, 433, 45
- Saxton, C. J., Sutherland R. S., & Bicknell G. V., 2001, ApJ, 563, 103
- Robinson D.C., 1971, Plasma Physics, 13, 439
- Ryu D., Kang H., & Biermann P. L., 1998, Astron.Astroph., 335, 19
- Schopper R, Birk G.T. & Lesch H., 2002, Astropart.Phys., 17, 347
- Takeda M. et al., 2003, Astropart. Phys., 19, 447
- Taylor J.B., 1986, Rev. Mod. Phys., 58, 741
- Taylor J.B., 1963, Phys. Fluids, 6, 1529
- Voslamber D. & Callebaut D.K., 1962, Phys. Rev., 128, 2016
- Wise M.W., McNamara B.R., Nulsen P.E.J., Houck J.C., & David L.P., 2007, ApJ, 659, 1153
- Yamamoto T., for the Pierre Auger Collaboration, 2007, 30th International Cosmic Ray Conference, Merida Mexico, July 2007, in press. arXiv:0707.2638v3 [astro-ph]
- Zatsepin G.T., Kuzmin V.A, 1966, JETP Lett., 4, 78